

Wigner Analysis of Particle Dynamics in Wide Nonharmonic Potentials

Andreu Riera-Campenya^{1,2}, Marc Roda-Llordes^{1,2}, Piotr T. Grochowski^{1,2,3}, and Oriol Romero-Isart^{1,2}

¹Institute for Quantum Optics and Quantum Information of the Austrian Academy of Sciences, A-6020 Innsbruck, Austria

²Institute for Theoretical Physics, University of Innsbruck, A-6020 Innsbruck, Austria

³Center for Theoretical Physics, Polish Academy of Sciences, Aleja Lotników 32/46, 02-668 Warsaw, Poland

We derive an analytical expression of a Wigner function that approximately describes the time evolution of the one-dimensional motion of a particle in a nonharmonic potential. Our result provides an excellent approximation in the regime of wide potentials and small fluctuations, namely potentials that enable spatial expansions orders of magnitude larger than the one of the initial state but that remain smaller compared to the relevant dynamical length scale (e.g., distance between turning points). Our analytical result elucidates the interplay between classical and quantum physics and the impact of decoherence during nonlinear dynamics. This analytical result is instrumental to design, optimize and understand proposals using nonlinear dynamics to generate macroscopic quantum states of massive particles.

1 Introduction

The one-dimensional position and momentum of a particle is perhaps the most fundamental degree of freedom in physics and of paramount importance in the development of quantum mechanics [1–3]. The state of such a continuous-variable degree of freedom can be described by the Wigner function [4–6], a phase-space quasi-probability distribution. The Wigner function and its time evolution allow us to study the interplay between classical and quantum mechanics as well as the impact of noise and decoherence [7–11]. Usually, the dynamics of the Wigner function are studied in scenarios of small phase-space areas, i.e., scenarios where the phase-space surface occupied by the initial state is of the same order as the space available to be explored through the dynamics. This is certainly the case for quantum experiments performed with photons [12–14] and atomic systems [15, 16], whose state, even at near-zero temperatures, is delocalized over scales comparable to the length scale of the confining potential. Motivated by recent experimental progress in controlling the quantum center-of-mass motion of a single nanoparticle [17–24], which has approximately nine orders of magnitude more mass than a single atom, here we focus on the rather unexplored regime of large-scale quantum dynamics. That is, the dynamics generated when a highly localized phase-space probability distribution evolves in a wide, nonharmonic potential that enables the particle to explore an orders-of-magnitude larger phase-space area.

In particular, in this paper, we provide an analytical expression for the time evolution of the Wigner function evolving in a nonharmonic potential, in the presence of decoherence

caused by weak coupling to a high-temperature bath [25–27], and white-noise fluctuations in both the amplitude and position of the potential [28–30]. We will show that this analytical expression provides an excellent approximation to the generated nonlinear open dynamics in the regime of (i) wide potentials, where the potential has a relevant length scale that is much larger than the initial spatial extent of the particle’s position, and (ii) small fluctuations, where the spatial delocalization of the particle’s state generated during the dynamics is much smaller than the potential length scale. Our results are timely as they synergize with recently developed numerical tools [31] that allow to design, optimize, and understand protocols where a quantum ground-state-cooled nanoparticle in a wide nonharmonic potential rapidly evolves into a macroscopic quantum superposition state [32].

The rest of the paper is organized as follows. In Sec. 2, we derive an analytical approach using Wigner analysis to describe the dynamics of a particle in a nonharmonic potential. We define the regime in which a key approximation, referred to as the constant-angle approximation, is used to integrate the nonlinear dynamics, thereby providing an analytical form of the time-evolved Wigner function. In Sec. 3, we apply our analytical method to the example of a particle evolving in a wide double-well potential. We explicitly show how our analytical approach reproduces the numerical results obtained using the split-method operator [33] and Q-Xpanse [31]. We draw our conclusions in Sec. 4 and provide further details of our analysis in the Appendix.

2 Wigner Analysis of Particle Nonlinear Dynamics

In this Section, we provide an analytical treatment of the one-dimensional dynamics of a particle evolving in a nonharmonic potential in the presence of decoherence. Initially (Sec. 2.1), we will delve into the detailed description of the dynamical problem under study, presenting both the Liouville-von Neumann equation and the equation of motion of the Wigner function. Subsequently, we will conduct two frame transformations that are exact: the classical centroid frame transformation (Sec. 2.2), and the Gaussian frame transformation (Sec. 2.3). These two transformations yield a valuable, exact reformulation of the dynamical problem. Following this, we will perform two approximations (Sec. 2.4): the constant-angle approximation and the linearized-decoherence approximation. These will lead to an easily evaluable expression of the time-evolved Wigner function. Finally, in Sec. 2.5, we will discuss the regime where we expect the constant-angle approximation to provide an accurate description of the nonlinear particle dynamics.

2.1 Description of the dynamical problem

We consider the one-dimensional dynamics of a particle with mass m , where the position and momentum operators are given by \hat{X} and \hat{P} , respectively, and they fulfill the canonical commutation rule $[\hat{X}, \hat{P}] = i\hbar$. The particle evolves under a potential denoted by $V(\hat{X})$, and in the presence of decoherence. The time evolution of the particle’s state, specified by its density operator $\hat{\rho}(t)$, is governed by the Liouville-von Neumann equation:

$$\frac{\partial}{\partial t} \hat{\rho}(t) = \frac{1}{i\hbar} \left[\frac{\hat{P}^2}{2m} + V(\hat{X}), \hat{\rho}(t) \right] + \mathcal{D}[\hat{\rho}(t)], \quad (1)$$

Here, $\mathcal{D}[\cdot]$ represents the decoherence superoperator, which we specify below. We are interested in studying the evolution of a particle that is initially cooled to a low-temperature thermal state in a harmonic potential of frequency Ω (for example, an optical trap). At zero

temperature, the particle has zero-point fluctuations, with $X_\Omega = \sqrt{\hbar/(2m\Omega)}$ in position, and $P_\Omega = \hbar/(2X_\Omega)$ in momentum.

Motivated by experiments with levitated nanoparticles in ultra-high vacuum [17–24, 34], we will model the decoherence as follows. First, we consider position localization decoherence [35–37], which is defined by the dissipator:

$$\mathcal{D}_{loc}[\circ] = -\frac{\Gamma_{loc}}{2X_\Omega^2}[\hat{X}, [\hat{X}, \circ]], \quad (2)$$

where Γ_{loc} is the position localization decoherence rate. This type of decoherence emerges in the weak-coupling high-temperature limit of Brownian motion [25–27, 38] as well as after performing an ensemble average of a white-noise stochastic force [39]. This decoherence model mimics the recoil heating due to laser light [40, 41] and the emission of thermal photons [36, 42–44], among other sources of decoherence. Additionally, we take into account the decoherence due to fluctuations in the potential’s center and its amplitude [28–30]. In particular, we consider the fluctuating potential:

$$V_{fluc}(X, t) = (1 + \xi_2(t))V(X - X_\Omega\xi_1(t)) \approx V(X) + \xi_1(t)X_\Omega V^{(1)}(X) + \xi_2(t)V(X), \quad (3)$$

where $\xi_1(t)$ and $\xi_2(t)$ are zero-average stochastic processes representing fluctuations of the potential’s center and amplitude, respectively. In Eq. (3), we have assumed small potential fluctuations, which justify the use of a Taylor series expansion in each $\xi_i(t)$, truncated to the first order. Also, we use the short-hand notation $V^{(n)}(X)$ to denote the n^{th} derivative of V with respect to its argument X , evaluated at X . For simplicity, we assume $\xi_i(t)$ to be independent Gaussian white noise processes with the correlation function $\langle\langle \xi_i(t)\xi_j(t') \rangle\rangle = 2\pi A_i\delta_{ij}\delta(t-t')$, where $\langle\langle \circ \rangle\rangle$ denotes the average over trajectories and A_i is a measure of the noise amplitude. The average over these stochastic processes can be computed using the cumulant expansion method to the second order [45], and leads to the decoherence superoperator:

$$\mathcal{D}_{fluc}[\circ] = -\frac{\pi A_1 X_\Omega^2}{\hbar^2}[V^{(1)}(\hat{X}), [V^{(1)}(\hat{X}), \circ]] - \frac{\pi A_2}{\hbar^2}[V(\hat{X}), [V(\hat{X}), \circ]]. \quad (4)$$

Putting everything together, the decoherence model used in this paper is given by $\mathcal{D}[\circ] = \mathcal{D}_{loc}[\circ] + \mathcal{D}_{fluc}[\circ]$. This dissipator can be compactly written as:

$$\mathcal{D}[\circ] = -\sum_{n,m=1}^{\infty} \frac{\Gamma_{nm}}{2X_\Omega^{n+m}}[\hat{X}^n, [\hat{X}^m, \circ]] \equiv \sum_{n,m=1}^{\infty} \mathcal{D}_{nm}[\circ]. \quad (5)$$

This form is obtained by performing a Taylor expansion of the potential, i.e., $V(X) = \sum_{n=1}^{\infty} V^{(n)}(0)X^n/n!$. The expression of the decoherence rates Γ_{nm} can be obtained by collecting the corresponding terms from $\mathcal{D}_{loc}[\circ]$ and $\mathcal{D}_{fluc}[\circ]$, and they are explicitly given in App. A. It should be noted that the dissipator $\mathcal{D}_{nm}[\circ]$ for n or m strictly larger than one, which originates from the potential fluctuations $\mathcal{D}_{fluc}[\circ]$, generates non-Gaussian dissipative dynamics.

We chose to use the Wigner function formalism [4, 5] to analytically handle the dynamics generated by Eq. (1). Moreover, we use the dimensionless position $x = X/X_\Omega$, momentum $p = P/P_\Omega$, and time $\tau = \omega t$ variables, where ω is an arbitrary frequency scale associated with the potential $V(X)$. The corresponding dimensionless potential in these units is defined as $U(x) \equiv V(xX_\Omega)/(m\omega^2 X_\Omega^2)$. In accordance with Eq. (1), the equation of motion for the dimensionless Wigner function $W(\mathbf{r}, \tau)$ is given by

$$\frac{\partial}{\partial \tau} W(\mathbf{r}, \tau) = (\mathcal{L}_c + \mathcal{L}_q + \mathcal{L}_d) W(\mathbf{r}, \tau), \quad (6)$$

where $\mathbf{r} \equiv (x, p)^\top$ denotes a point in the dimensionless phase space. The first term generates classical (i.e., Liouville) dynamics and is expressed as:

$$\mathcal{L}_c = -\frac{\Omega}{\omega} p \frac{\partial}{\partial x} + \frac{\omega}{\Omega} U^{(1)}(x) \frac{\partial}{\partial p}. \quad (7)$$

The second term generates genuine quantum dynamics and is written as:

$$\mathcal{L}_q = \frac{\omega}{\Omega} \sum_{n=1}^{\infty} (-1)^n \frac{U^{(2n+1)}(x)}{(2n+1)!} \left(\frac{\partial}{\partial p} \right)^{2n+1}. \quad (8)$$

Note that $\mathcal{L}_c + \mathcal{L}_q$ generates the same evolution as the Schrödinger equation, and that $\mathcal{L}_q = 0$ for up to quadratic potentials. Lastly, the third term generates decoherence, which in accordance with Eq. (5), can be written as $\mathcal{L}_d = \sum_{n,m=1}^{\infty} \mathcal{L}_{d,nm}$, where:

$$\mathcal{L}_{d,nm} = \sum_{k=2}^{n+m} c_{nmk} x^{n+m-k} \left(\frac{\partial}{\partial p} \right)^k. \quad (9)$$

The specific expression of the coefficients c_{nmk} is provided in App. A. Note that while we have focused on the one-dimensional motion of massive particles, our results, especially when written in this dimensionless form, can be applied to describe the nonlinear dynamics of other continuous-variable degrees of freedom (e.g., a single electromagnetic field mode).

The aim of this paper is to solve Eq. (6) for an initial Gaussian state, whose Wigner function can be written as:

$$W(\mathbf{r}, 0) = G[\mathbf{C}(0)](\mathbf{r} - \boldsymbol{\mu}(0)). \quad (10)$$

Here, $G[\mathbf{C}](\mathbf{r})$ denotes the two-dimensional Gaussian distribution:

$$G[\mathbf{C}](\mathbf{r}) \equiv \frac{1}{2\pi \det \mathbf{C}} \exp\left(-\frac{\mathbf{r}^\top \mathbf{C}^{-1} \mathbf{r}}{2}\right), \quad (11)$$

and $\boldsymbol{\mu}(0) = (\langle \hat{x} \rangle(0), \langle \hat{p} \rangle(0))^\top$ and $\mathbf{C}(0)$ refer to the initial mean values and the covariance matrix of $\hat{\rho}(0)$, respectively. The elements $C_{ij}(0)$, where $i, j \in \{x, p\}$, of the always symmetric covariance matrix, are given by:

$$C_{ij}(0) = \frac{1}{2} \langle \hat{r}_i \hat{r}_j + \hat{r}_j \hat{r}_i \rangle(0) - \langle \hat{r}_i \rangle(0) \langle \hat{r}_j \rangle(0). \quad (12)$$

For instance, a thermal state with a mean phonon occupation number \bar{n} serves as a particularly relevant initial state, which corresponds to $\mathbf{C}(0) = (2\bar{n}+1)\mathbf{1}_2$, being $\mathbf{1}_2$ the two-by-two identity matrix.

In the following section, we will derive an expression for $W(\mathbf{r}, \tau)$, which approximately solves Eq. (6). We obtain this expression by performing two consecutive frame transformations (i.e., the classical centroid frame and the Gaussian frame) and applying a key approximation, namely the constant-angle approximation. We will further simplify this expression using the linearized-decoherence approximation.

2.2 Classical centroid frame

The first frame transformation aims to remove the dynamics of the mean position and momentum values, effectively moving to a comoving frame that aligns with the approximate

centroid of the Wigner function [46]. To achieve this, we define $W_c(\tau) \equiv M_c(\tau)^{-1}W(\mathbf{r}, \tau)$, where $M_c(\tau)$ is a time-dependent phase-space displacement map, expressed as:

$$M_c(\tau) \equiv \exp \left[-\mathbf{r}_c(\tau)^\top \nabla \right] = \exp \left[-x_c(\tau) \frac{\partial}{\partial x} - p_c(\tau) \frac{\partial}{\partial p} \right]. \quad (13)$$

where $\nabla = (\partial/\partial x, \partial/\partial p)^\top$ is the phase space gradient. In Eq. (13), $\mathbf{r}_c(\tau) \equiv (x_c(\tau), p_c(\tau))^\top$ represents the classical centroid trajectory, which is the solution to dimensionless Hamilton's equations

$$\frac{\partial}{\partial \tau} x_c(\tau) = \frac{\Omega}{\omega} p_c(\tau), \quad (14)$$

$$\frac{\partial}{\partial \tau} p_c(\tau) = -\frac{\omega}{\Omega} U^{(1)}(x_c(\tau)), \quad (15)$$

with initial conditions given by $\mathbf{r}_c(0) = (x_c(0), p_c(0))^\top = (\langle \hat{x} \rangle(0), \langle \hat{p} \rangle(0))^\top$. The action of the map $M_c(\tau)$ on an arbitrary function $f(\mathbf{r})$ translates its phase-space variables as $M_c(\tau)f(\mathbf{r}) = f(\mathbf{r} - \mathbf{r}_c(\tau))$. In this frame, we describe the dynamics of the Wigner function centered at the classical trajectory that is followed by its initial position and momentum expected value. This frame transformation does not imply any approximation. It will be particularly useful for nonlinear dynamics that maintain a small distance between the vector $\mathbf{r}_c(\tau) = (x_c(\tau), p_c(\tau))^\top$ and $\boldsymbol{\mu}(\tau) = (\langle \hat{x} \rangle(\tau), \langle \hat{p} \rangle(\tau))^\top$ in comparison to the available phase-space dimensions. As we will demonstrate later, this will be the case for wide potentials and small fluctuations.

In this classical centroid frame, one can show that the state $W_c(\mathbf{r}, \tau)$ evolves according to an effective time-dependent potential, represented by

$$U_{\text{eff}}(x, \tau) \equiv \sum_{n=2}^{\infty} \frac{1}{n!} U^{(n)}(x_c(\tau)) x^n. \quad (16)$$

This effective potential, at least quadratic in position, exhibits time-dependence determined by the local derivatives of the potential along the classical trajectory. Thus, in the comoving frame with the approximate centroid of the Wigner function, the particle experiences a time-dependent potential while traversing the static potential. More specifically, the evolution equation for $W_c(\mathbf{r}, \tau)$ can be expressed as:

$$\frac{\partial}{\partial \tau} W_c(\mathbf{r}, \tau) = \left[\mathcal{L}_c^c(\tau) + \mathcal{L}_q^c(\tau) + \mathcal{L}_d^c(\tau) \right] W_c(\mathbf{r}, \tau), \quad (17)$$

Here, $\mathcal{L}_c^c(\tau)$ and $\mathcal{L}_q^c(\tau)$ are defined by replacing $U(x)$ with $U_{\text{eff}}(x, \tau)$ in Eq. (7) and Eq. (8), respectively. The generator of decoherence also becomes time-dependent and is given by $\mathcal{L}_d^c(\tau) \equiv M_c(\tau)^{-1} \mathcal{L}_d M_c(\tau) = \sum_{n,m=1}^{\infty} \mathcal{L}_{d,nm}^c(\tau)$, with

$$\mathcal{L}_{d,nm}^c(\tau) = \sum_{k=2}^{n+m} c_{nmk} [x + x_c(\tau)]^{n+m-k} \left(\frac{\partial}{\partial p} \right)^k. \quad (18)$$

2.3 Gaussian frame

The second frame transformation aims to remove the conservative Gaussian (i.e., linear) dynamics generated by the harmonic part of the effective potential Eq. (16), which we define as:

$$U_g(x, \tau) \equiv \frac{1}{2} \alpha(\tau) x^2. \quad (19)$$

Here, $\alpha(\tau) \equiv U^{(2)}(x_c(\tau))$ represents an effective (dimensionless) spring constant, which can be either positive or negative. To remove the Gaussian conservative dynamics, we define $W_g(\mathbf{r}, \tau) \equiv M_g(\tau)^{-1}W_c(\mathbf{r}, \tau)$, where $M_g(\tau)$ is given by:

$$M_g(\tau) \equiv \exp_+ \left[\int_0^\tau d\tau' \mathcal{L}_g(\tau') \right], \quad (20)$$

In this case, $\exp_+(\circ)$ represents the time-ordered exponential of the generator of Gaussian conservative dynamics, defined as:

$$\mathcal{L}_g(\tau) = -\frac{\Omega}{\omega} p \frac{\partial}{\partial x} + \frac{\omega}{\Omega} U_g^{(1)}(x, \tau) \frac{\partial}{\partial p}. \quad (21)$$

The generator of conservative non-Gaussian dynamics [47], attributed to the nonharmonic terms of the static potential, is given by $\mathcal{L}_{ng}(\tau) \equiv \mathcal{L}_c^c(\tau) + \mathcal{L}_q^c(\tau) - \mathcal{L}_g(\tau)$.

The map $M_g(\tau)$ generates Gaussian conservative physics, namely squeezing and phase-space rotations. Its action on an arbitrary function $f(\mathbf{r})$ is $M_g(\tau)f(\mathbf{r}) = f(\mathbf{S}(\tau)^{-1}\mathbf{r})$, where $\mathbf{S}(\tau)$ is a symplectic matrix. The matrix $\mathbf{S}(\tau)$ is obtained as the solution to the differential equation

$$\frac{\partial}{\partial \tau} \mathbf{S}(\tau) = \begin{pmatrix} 0 & \Omega/\omega \\ -(\omega/\Omega)\alpha(\tau) & 0 \end{pmatrix} \mathbf{S}(\tau), \quad (22)$$

with the initial condition $\mathbf{S}(0) = \mathbf{1}_2$. One can verify that $\det[\mathbf{S}(\tau)] = 1$ for all τ , and therefore, denoting $S_{ij}(\tau)$, with $i, j \in \{x, p\}$ as the components of $\mathbf{S}(\tau)$, its inverse is given by

$$\mathbf{S}(\tau)^{-1} = \begin{pmatrix} S_{pp}(\tau) & -S_{xp}(\tau) \\ -S_{px}(\tau) & S_{xx}(\tau) \end{pmatrix}. \quad (23)$$

Importantly, the action of the map $M_g(\tau)$ on the phase space variable x is given by

$$M_g(\tau)^{-1}xM_g(\tau) \equiv \eta(\tau)x_{\varphi(\tau)} = \eta(\tau)[\cos(\varphi(\tau))x + \sin(\varphi(\tau))p], \quad (24)$$

where $\mathbf{r}_{\varphi(\tau)} \equiv \mathbf{R}[\varphi(\tau)]\mathbf{r} = (x_{\varphi(\tau)}, p_{\varphi(\tau)})^\top$ are rotated phase-space variables according to the rotation matrix

$$\mathbf{R}[\varphi(\tau)] \equiv \begin{pmatrix} \cos[\varphi(\tau)] & \sin[\varphi(\tau)] \\ -\sin[\varphi(\tau)] & \cos[\varphi(\tau)] \end{pmatrix}, \quad (25)$$

and we have defined the two key variables

$$\eta(\tau) \equiv \sqrt{S_{xx}(\tau)^2 + S_{xp}(\tau)^2}, \quad (26)$$

$$\tan[\varphi(\tau)] \equiv \frac{S_{xp}(\tau)}{S_{xx}(\tau)}. \quad (27)$$

Similar transformation rules can be derived for $\partial/\partial p$, involving the same functions $\eta(\tau)$ and $\varphi(\tau)$, and for p and $\partial/\partial x$ using similar functions that combine $S_{pp}(\tau)$ and $S_{px}(\tau)$ instead of $S_{xx}(\tau)$ and $S_{xp}(\tau)$. In summary, the map $M_g(\tau)$ generates time-dependent phase-space rotations with an angle $\varphi(\tau)$ and time-dependent squeezing with a squeezing parameter $\eta(\tau)$.

In the centroid and Gaussian frame, the evolution equation of $W_g(\mathbf{r}, \tau)$ is given by

$$\frac{\partial}{\partial \tau} W_g(\mathbf{r}, \tau) = \left[\mathcal{L}_{ng}^g(\tau) + \mathcal{L}_d^g(\tau) \right] W_g(\mathbf{r}, \tau), \quad (28)$$

where $\mathcal{L}_{ng}^g(\tau) \equiv M_g(\tau)^{-1} \mathcal{L}_{ng}(\tau) M_g(\tau)$ and $\mathcal{L}_d^g(\tau) \equiv M_g(\tau)^{-1} \mathcal{L}_d^c(\tau) M_g(\tau) = \sum_{n,m=1}^{\infty} \mathcal{L}_{d,nm}^g$. The explicit form of the generator of conservative non-Gaussian dynamics is given by

$$\mathcal{L}_{ng}^g(\tau) = \sum_{n=2}^{\infty} \beta_{n+1}(\tau) x_{\varphi(\tau)}^n \frac{\partial}{\partial p_{\varphi(\tau)}} + \sum_{\substack{n=1 \\ m=0}}^{\infty} (-1)^n \binom{2n+m}{m} \frac{\beta_{2n+m+1}(\tau)}{2n+1} x_{\varphi(\tau)}^m \left(\frac{\partial}{\partial p_{\varphi(\tau)}} \right)^{2n+1}, \quad (29)$$

where the first and second term account for classical and quantum non-Gaussian dynamics, respectively, and we have defined

$$\beta_n(\tau) \equiv \frac{\omega}{\Omega} \frac{U^{(n)}(x_c(\tau))}{(n-1)!} \eta(\tau)^n. \quad (30)$$

Note that the magnitude of the parameters $\beta_n(\tau)$ will determine whether non-Gaussian dynamics are generated. This shows that large squeezing, that is, a large value of $\eta(\tau)$, enhances the effect of the nonharmonicities in the potential. The specific form of the generators of decoherence is given by

$$\mathcal{L}_{d,nm}^g(\tau) = \sum_{k=2}^{n+m} c_{nmk} \left[\eta(\tau) x_{\varphi(\tau)} + x_c(\tau) \right]^{n+m-k} \eta(\tau)^k \left(\frac{\partial}{\partial p_{\varphi(\tau)}} \right)^k. \quad (31)$$

Note that decoherence is also enhanced by squeezing.

We emphasize that up to this point, the analytical approach is exact; that is, no approximations have been made. We have, however, singled out the challenging part of solving a nonlinear open quantum dynamical problem, which is to integrate Eq. (28) with the initial condition given by $W_g(\mathbf{r}, 0) = M_g(0)^{-1} M_c(0)^{-1} W(\mathbf{r}, 0)$. If one obtains $W_g(\mathbf{r}, \tau)$, the exact solution of Eq. (6) is given by

$$W(\mathbf{r}, \tau) = M_c(\tau) M_g(\tau) W_g(\mathbf{r}, \tau). \quad (32)$$

As we show below, this exact reformulation of the problem allows us to identify a key approximation that provides an approximated expression for $W_g(\mathbf{r}, \tau)$, which is significantly easier to calculate.

2.4 Constant-angle and linearized-decoherence approximation

Ultimately, the reason a closed form solution for $W_g(\mathbf{r}, \tau)$ is not possible stems from the fact that the angle $\varphi(\tau)$ changes over time. This results in the generators $\mathcal{L}_{ng}^g(\tau)$ and $\mathcal{L}_d^g(\tau)$ being noncommutative with themselves at different times. This fact motivates the use of the constant-angle approximation, which involves replacing $\varphi(\tau)$ with a given constant-angle ϕ , in $\mathcal{L}_{ng}^g(\tau)$ and $\mathcal{L}_d^g(\tau)$. Under this approximation, the generator of Eq. (28) commutes with itself at different times, and furthermore, all its summands also commute with each other. We will first implement this approximation and then, in the subsequent subsection, discuss the regime where we expect it to provide an accurate description of the particle's nonlinear dynamics.

Within the constant-angle approximation, the approximated solution of $W_g(\mathbf{r}, \tau)$ is given by an exponential map (rather than a time-ordered exponential one), which can be factorized, and its coefficients are time-dependent. This can be expressed as follows:

$$W_g(\mathbf{r}, \tau) \approx M_{ng}(\tau) D_{ng}(\tau) W_g(\mathbf{r}, 0). \quad (33)$$

Here, $M_{ng}(\tau)$ generates non-Gaussian conservative dynamics and is given by the exponential map $M_{ng}(\tau) = \exp[\Lambda_{ng}(\tau)]$, where

$$\Lambda_{ng}(\tau) \equiv \sum_{n=2}^{\infty} \kappa_{n+1}(\tau) x_{\phi}^n \frac{\partial}{\partial p_{\phi}} + \sum_{\substack{n=1 \\ m=0}}^{\infty} (-1)^n \binom{2n+m}{m} \frac{\kappa_{2n+m+1}(\tau)}{2n+1} x_{\phi}^m \left(\frac{\partial}{\partial p_{\phi}} \right)^{2n+1}. \quad (34)$$

The first and second terms account for classical and quantum non-Gaussian dynamics, respectively. The time-dependent coefficients quantifying the strength of the generator of these conservative non-Gaussian dynamics are given by

$$\kappa_n(\tau) \equiv \int_0^{\tau} d\tau' \beta_n(\tau') = \frac{\omega}{\Omega} \int_0^{\tau} d\tau' \frac{U^{(n)}(x_c(\tau'))}{(n-1)!} \eta(\tau')^n. \quad (35)$$

The generation of decoherence is given by the exponential map $D_{ng}(\tau) \equiv \exp[\Lambda_d(\tau)]$, where

$$\Lambda_d(\tau) \equiv \int_0^{\tau} d\tau' \sum_{n,m=1}^{\infty} \sum_{k=2}^{n+m} c_{nmk} x_c(\tau')^{n+m} \left[1 + \frac{\eta(\tau')}{x_c(\tau')} x_{\phi} \right]^{n+m-k} \left[\frac{\eta(\tau')}{x_c(\tau')} \right]^k \left(\frac{\partial}{\partial p_{\phi}} \right)^k. \quad (36)$$

Note that by using the constant-angle approximation, the solution to the dynamics in Wigner space has been significantly simplified. This is because one has replaced the integration of a complicated partial differential equation with the more efficient integration of a set of time-dependent functions.

In addition to the constant-angle approximation, a second approximation can be performed on the decoherence map under the assumption of small fluctuations. This means that the following condition is met:

$$\frac{\eta(\tau)}{x_c(\tau)} \ll 1. \quad (37)$$

This is the regime in which the position fluctuations of the particle are smaller than its mean value. In the case where $x_c(\tau) = 0$, the linearization of the decoherence generator may still be possible, albeit for different underlying reasons. Under this regime, one can perform the linearized-decoherence approximation, which consists of expanding Eq. (36) in powers of $\eta(\tau)/x_c(\tau)$ and keeping the lowest order terms up to the second order. The lowest-order terms can be written compactly as follows:

$$\Lambda_d(\tau) \approx \Lambda_d^a(\tau) \equiv \frac{\sigma_b(\tau)^2}{2} \left(\frac{\partial}{\partial p_{\phi}} \right)^2. \quad (38)$$

The time-dependent parameter $\sigma_b(\tau)$ quantifies the strength of decoherence and is given by

$$\sigma_b(\tau)^2 \equiv 4 \int_0^{\tau} d\tau' \frac{\Gamma_{eff}(\tau')}{\omega} \eta(\tau')^2. \quad (39)$$

The effective time-dependent decoherence rate is given by $\Gamma_{eff}(\tau) \equiv \Gamma_{loc} + \Gamma_{fluc}(\tau)$, with the contribution arising from the trap fluctuations

$$\frac{\Gamma_{fluc}(\tau)}{\Omega} = \frac{\pi\omega^4 A_1}{2\Omega^3} \left([U^{(2)}(x_c(t))]^2 + \frac{A_2}{A_1} [U^{(1)}(x_c(t))]^2 \right). \quad (40)$$

Note that this approximation corresponds to linearizing the decoherence generator $\mathcal{L}_d^g(\tau) = \sum_{n,m=1}^{\infty} \mathcal{L}_{d,nm}^g(\tau)$ in Eq. (31), which can be approximated as:

$$\mathcal{L}_d^g(\tau) \approx \mathcal{L}_d^{g,a}(\tau) \equiv \frac{2\Gamma_{\text{eff}}(\tau)}{\omega} \eta(\tau)^2 \left(\frac{\partial}{\partial p_\phi} \right)^2. \quad (41)$$

Putting everything together, the constant-angle and linearized-decoherence approximation allows us to obtain an approximate solution of the open nonlinear quantum mechanical problem described by Eq. (6). This can be represented as follows:

$$W_a(\mathbf{r}, \tau) = M_c(\tau)M_g(\tau)M_{ng}(\tau)D_g(\tau)W_g(\mathbf{r}, 0) \quad (42)$$

$$= D(\tau)M_c(\tau)M_g(\tau)M_{ng}(\tau)W_g(\mathbf{r}, 0), \quad (43)$$

Here, we have defined $D_g(\tau) \equiv \exp[\Lambda_d^a(\tau)]$ and $D(\tau) \equiv M_g(\tau)D_g(\tau)M_g(\tau)^{-1}$. Also, recall that $W_g(\mathbf{r}, 0) = M_g(0)^{-1}M_c(0)^{-1}W(\mathbf{r}, 0)$. In the second equation, we have used the fact that $D_g(\tau)$ commutes with $M_{ng}(\tau)$ and $D(\tau)$ with $M_c(\tau)$. The expression in the second equation is particularly convenient as the decoherence map is applied to the coherently evolved state. In this case, the decoherence map is given by:

$$D(\tau) \equiv \exp \left[\frac{\nabla^\top \mathbf{C}_b(\tau) \nabla}{2} \right], \quad (44)$$

where

$$\mathbf{C}_b(\tau) = \sigma_b(\tau)^2 \mathbf{S}(\tau) \mathbf{R}(\phi)^\top (\mathbf{e}_p \mathbf{e}_p^\top) \mathbf{R}(\phi) \mathbf{S}(\tau)^\top \quad (45)$$

is the blurring covariance matrix and $\mathbf{e}_p = (0, 1)^\top$ is a unit vector along the momentum component. The action of the decoherence map $D(\tau)$ corresponds to a convolution with a Gaussian distribution of covariance matrix $\mathbf{C}_b(\tau)$, namely:

$$D(\tau)f(\mathbf{r}) = \int d\mathbf{r}' G[\mathbf{C}_b(\tau)](\mathbf{r} - \mathbf{r}') f(\mathbf{r}'). \quad (46)$$

Here, the Gaussian distribution $G[\mathbf{C}](\mathbf{r})$ is defined as per Eq. (11). Physically, $\sigma_b(\tau)$ determines the smallest length scale that remains unaffected by decoherence and is sometimes referred to as the blurring distance [48–50].

We can now use the expression $W_a(\mathbf{r}, \tau)$ in Eq. (43) to calculate the first and second moments. As shown in App. B.1 and B.2, the first moments $\boldsymbol{\mu}_a(\tau)$ can be expressed as

$$\boldsymbol{\mu}_a(\tau) = \mathbf{r}_c(\tau) - \mathbf{S}(\tau) \mathbf{R}(\phi)^\top \mathbf{e}_p \sum_{n \geq 3} \kappa_n(t) \langle \hat{x}_\phi^{n-1} \rangle_g(0). \quad (47)$$

where $\langle \circ \rangle_g(\tau)$ is the average in the centroid and Gaussian frame; that is, computed with $W_g(\mathbf{r}, \tau)$. Note that the first moments are not affected by decoherence. The second moments, namely the covariance matrix evaluated using $W_a(\mathbf{r}, \tau)$, can be expressed as

$$\begin{aligned} \mathbf{C}_a(\tau) = & \mathbf{C}_b(\tau) + \mathbf{S}(\tau) \mathbf{R}(\phi)^\top \left[\mathbf{C}(0) - \sum_{n \geq 3} \kappa_n(t) \begin{pmatrix} 0 & \langle \hat{x}_\phi^n \rangle_g(0) \\ \langle \hat{x}_\phi^n \rangle_g(0) & \langle \hat{x}_\phi^{n-1} \hat{p}_\phi \rangle_g(0) \end{pmatrix} \right. \\ & \left. + \sum_{n, m \geq 3} \kappa_n(t) \kappa_m(t) \begin{pmatrix} 0 & 0 \\ 0 & \langle \hat{x}_\phi^{n+m-2} \rangle_g(0) - \langle \hat{x}_\phi^{n-1} \rangle_g(0) \langle \hat{x}_\phi^{m-1} \rangle_g(0) \end{pmatrix} \right] \mathbf{R}(\phi) \mathbf{S}(\tau)^\top. \quad (48) \end{aligned}$$

Note that the decoherence appears in the covariance matrix through the addition of the blurring covariance matrix defined in Eq. (45). Nonlinear dynamics are manifested by the dependence of $\mathbf{C}_a(\tau)$ on the initial moments higher than the second [51]. In the next section, we argue that the accuracy of $\boldsymbol{\mu}_a(\tau)$ and $\mathbf{C}_a(\tau)$ in approximating $\boldsymbol{\mu}(\tau)$ and $\mathbf{C}(\tau)$ is a useful measure of the merit of our analytical approach.

2.5 Validity of the constant-angle approximation

Our analytical approach relies on the *constant-angle* and *linearized-decoherence* approximations, which lead to the expression $W_a(\mathbf{r}, \tau)$, given in Eq. (43). We note that the linearized-decoherence approximation, performed after the constant-angle approximation, is convenient but not essential, and its validity is well characterized by the small-fluctuations condition in Eq. (37) for dynamics in which $x_c(\tau) \neq 0$. Regarding the constant-angle approximation, we need to compare how closely $W_a(\mathbf{r}, \tau)$ approximates the solution $W(\mathbf{r}, \tau)$. One can show that an upper bound for the norm of the difference of the exact and approximated Wigner functions is proportional to the function

$$\chi(\tau; \phi) \equiv \sum_{n \geq 3} \int_0^\tau d\tau' |\beta_n(\tau')| |\varphi(\tau') - \phi|. \quad (49)$$

Indeed, this quantity is minimized if the angle $\varphi(t)$ is constant and close to ϕ on the time scales where the nonharmonicities are large, namely when the $\beta_n(\tau)$ are large. In this context, it is useful to remember that the time derivative of the angle is given by

$$\frac{d}{d\tau} \varphi(\tau) = \frac{\Omega/\omega}{\eta(\tau)^2}, \quad (50)$$

indicating that large fluctuations, namely $\eta(\tau) \gg 1$, will make the angle more constant. Together with the small-fluctuations condition Eq. (37) required for the linearized-decoherence approximation, our analytical approach requires the regime $x_c(\tau) \gg \eta(\tau) \gg 1$ in the time scales where the generators of nonlinear dynamics cannot be neglected.

Ultimately, the best way to quantify the performance of our analytical approach is to compare $W_a(\mathbf{r}, \tau)$ with the numerically evaluated $W(\mathbf{r}, \tau)$. In this case, we suggest comparing observables rather than the overlap between the two states. The reason is that large-scale dynamics generate states with very small phase-space features, even sub-Planckian [10, 31] that can immediately provide a very low overlap if not captured accurately. These small features can nevertheless be irrelevant in capturing the observables of interest and may immediately disappear in the presence of unavoidable sources of noise and decoherence. Therefore, we suggest quantifying the performance of the constant-angle approximation by comparing global observable properties of the state such as their first and second moments. This can be done by evaluating their relative error, namely,

$$\epsilon_1(\tau) \equiv \frac{2\|\boldsymbol{\mu}(\tau) - \boldsymbol{\mu}_a(\tau)\|}{\|\boldsymbol{\mu}(\tau)\| + \|\boldsymbol{\mu}_a(\tau)\|}, \quad (51)$$

with the vector norm $\|\mathbf{y}\| = \sqrt{\mathbf{y}^\dagger \mathbf{y}}$, and

$$\epsilon_2(\tau) \equiv \frac{2\|\mathbf{C}(\tau) - \mathbf{C}_a(\tau)\|_2}{\|\mathbf{C}(\tau)\|_2 + \|\mathbf{C}_a(\tau)\|_2}, \quad (52)$$

where $\|\mathbf{A}\|_2 = \sqrt{\text{tr}(\mathbf{A}^\dagger \mathbf{A})}$ is the Hilbert-Schmidt norm. In summary, we recommend to evaluate $\chi(\tau; \phi)$, $\epsilon_1(\tau)$ and $\epsilon_2(\tau)$ to quantify the performance of the constant-angle approximation, something we will do in the example shown in the following section.

Finally, let us emphasize that around a turning point, say τ_m , the state is expected to compress, namely to minimize $\eta(\tau)$. Hence, according to Eq. (50), around a turning point the angle $\varphi(\tau)$ will not change slowly. By performing a Taylor expansion of $\varphi(\tau)$ around the time τ_m , recall Eq. (26), it follows that the time derivative of the angle around a compression time has a Lorentzian shape

$$\frac{d}{d\tau} \varphi(\tau) \approx \frac{\gamma(\tau_m)}{\gamma(\tau_m)^2 + (\tau - \tau_m)^2}, \quad (53)$$

with width $\gamma(\tau_m) \equiv (\omega/\Omega)\eta(\tau_m)^2$. Therefore, by integrating this Lorentzian, we see that around a turning point the angle should change approximately by π . This implies that if the constant-angle approximation is performed with an angle ϕ during the time scale before a turning point, a second angle around $\phi + \pi$ will need to be employed after the turning point. We will show and use this explicitly in the example provided in the following section.

3 Example: dynamics in a wide double-well potential

Let's demonstrate how the formalism developed in the previous section can be applied to describe the nonlinear dynamics of a particle using a relevant example. Inspired by a recent proposal to prepare a macroscopic quantum superposition of a levitated nanoparticle via the dynamics in a wide nonharmonic potential [32], we will focus on the double-well potential given by:

$$V_{dw}(X) = \frac{1}{2}m\omega^2 \left(-X^2 + \frac{X^4}{2D^2} \right). \quad (54)$$

This potential is characterized by the frequency ω and the distance scale D . To adapt the results of the previous section, we will employ the dimensionless potential:

$$U_{dw}(x) = \frac{1}{2} \left(-x^2 + \frac{x^4}{2d^2} \right), \quad (55)$$

where $D = dX_\Omega$. We will consider the wide-potential regime defined by $d \gg 1$. We consider the initial condition given by a thermal state of a harmonic potential of frequency Ω centered at $x = 0$ with phonon mean number occupation \bar{n} and mean position and momentum values denoted by $\boldsymbol{\mu}(0) = (\langle \hat{x} \rangle(0), \langle \hat{p} \rangle(0))^T = (x_s, 0)^T$, where $d \gg x_s \gg 1$, such that the dynamics are constrained to the right side of the double-well potential. Whenever necessary, we will utilize the parameters listed in Table 1, which correspond to the size L dynamics defined in [32].

To transition to the classical centroid frame, we need to evaluate the classical trajectory $\mathbf{r}_c(\tau) = (x_c(\tau), p_c(\tau))^T$ with $\mathbf{r}_c(0) = \boldsymbol{\mu}(0)$. This classical trajectory can be solved analytically [52, 53] using the Jacobi elliptic functions [54]. In Fig. 1a, we display the classical trajectory, which is periodic and has an *avocado* shape. The analytical solution allows us to obtain analytical expressions for the timescales governing the classical dynamics, which are solely functions of x_s/d . We will be particularly interested in the time scale

$$\tau_m = \log \left(4\sqrt{\frac{2d}{x_s}} + O(\sqrt{x_s/d}) \right), \quad (56)$$

which corresponds to the turning point of the classical trajectory of the centroid. It also corresponds to the half-period of the evolution, and the time at which the distance from the origin, given by $x_c(\tau_m) = \sqrt{2d^2 - x_s^2}$, reaches its maximum.

Parameter:	ω/Ω	d	x_s/d	\bar{n}
Value:	10^{-2}	10^4	10^{-1}	0

Table 1: Parameters used in the double-well potential example.

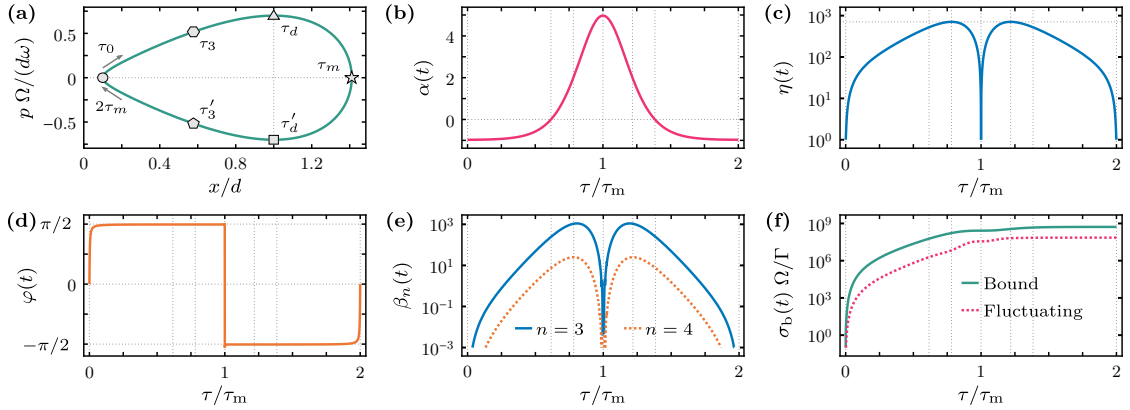


Figure 1: Relevant functions for our analytical approach computed for the parameters in Table 1. Panel (a) shows the classical trajectory $\mathbf{r}_c(\tau)$ in units of d . Panels (b),(c),(d),(e) and (f) show, respectively, $\alpha(\tau)$ (cf. Eq. (19)), $\eta(\tau)$ (Eq. (26)), $\varphi(\tau)$ (Eq. (27)), $\beta_n(\tau)$ (Eq. (30)), and $\sigma_b(\tau)\Omega/\Gamma$ (see Eq. (39)) both for the upper bounded and the fluctuating decoherence. The polygons in panel (a) indicate relevant instances of time, namely times when $\alpha(\tau)$ becomes zero ($\tau = \tau_3$), times when $\eta(\tau)$ is maximum ($\tau = \tau_d$) and the time half way through the classical trajectory ($\tau = \tau_m$). These instances of time appear as grid lines in the rest of the plots.

In the classical centroid frame, the effective potential from Eq. (16) becomes time-dependent. The harmonic part of this time-dependent effective potential, given by Eq. (19), has a dimensionless spring constant:

$$\alpha(\tau) = -1 + 3 \left(\frac{x_c(\tau)}{d} \right)^2, \quad (57)$$

which we illustrate in Fig. 1(b). Initially, this effective harmonic potential is inverted ($\alpha(\tau) < 0$) until the time τ_3 , which is defined by $x_c(\tau_3) = d/\sqrt{3}$. It then transforms into a harmonic potential ($\alpha(\tau) > 0$) until time $2\tau_m - \tau_3$, where it reverts to being inverted. This sequence of inverted, harmonic, and inverted potentials echoes the dynamics leveraged in the loop protocol proposed in [55].

Using the effective Harmonic potential, we can transition to the Gaussian frame. In this frame, we can compute both the squeezing rate $\eta(\tau)$ and angle $\varphi(\tau)$, which are depicted in Fig.1(c) and Fig.1(d), respectively. The state initially expands (i.e., squeezes) until it reaches a maximum at $\tau = \tau_d$, which for large Ω/ω is approximately given by

$$\eta_\star = \frac{1}{\sqrt{2}} \frac{\Omega x_s}{\omega d}. \quad (58)$$

The state then compresses (i.e., anti-squeezes) until the turning point τ_m . From here, the dynamics repeat until $2\tau_m$. Regarding the angle $\varphi(\tau)$, we observe the anticipated behavior discussed in Sec. 2.5, i.e., it remains constant (after the initial variation) until the first turning point, at which point it undergoes an approximated π -shift.

In the Gaussian frame, the strength of the nonlinear dynamics induced by the nonharmonicities in the potential is parameterized by the $\beta_n(\tau)$ ($n > 2$) variables, as given in Eq. (30). For the double-well potential, we have

$$\beta_3(\tau) = \frac{\omega}{\Omega d^2} 3x_c(\tau)\eta(\tau)^3, \quad (59)$$

$$\beta_4(\tau) = \frac{\omega}{\Omega d^2} \eta(\tau)^4. \quad (60)$$

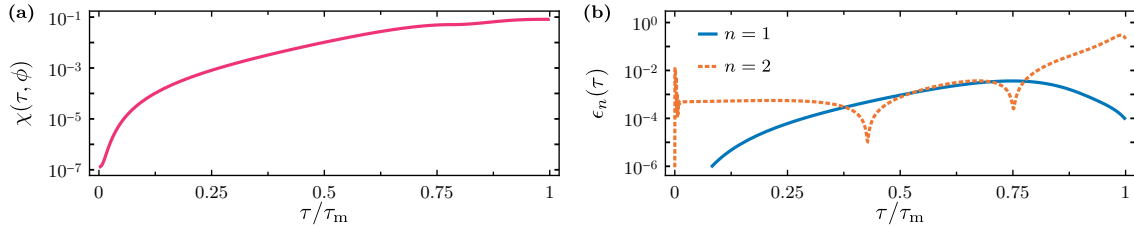


Figure 2: Quantities related to the validity of the constant-angle approximation for dynamics in a double-well with the parameters in Table 1. Panel (a) shows $\chi(\tau; \phi)$, and panel (b) shows the relative errors $\epsilon_1(\tau)$ (see Eq. (51)) and $\epsilon_2(\tau)$ (see Eq. (52)).

These variables are illustrated in Fig.1(e). They demonstrate how the strength of these nonlinearities is determined by the amount of squeezing $\eta(\tau)$, which can be compared with Fig.1(c). Furthermore, it is evident that the cubic nonlinearity is larger than the quartic nonlinearity in the small-fluctuations regime, denoted by $\eta(\tau) \ll x_c(\tau)$.

Regarding the impact of decoherence, the key variable within the linearized-decoherence approximation, which is valid within the regime $\eta(\tau) \ll x_c(\tau)$, is the blurring distance $\sigma_b(\tau)^2$, as shown in Eq. (39). The blurring distance depends on the effective time-dependent decoherence rate $\Gamma_{eff}(\tau) = \Gamma_{loc} + \Gamma_{fluc}(\tau)$, which includes the contribution from the potential's fluctuations as given in Eq. (40). For the case of the double-well potential where $x_c(\tau) < \sqrt{2}d$, $\Gamma_{fluc}(\tau)$ is upper bounded by the time-independent decoherence rate

$$\frac{\Gamma_{fluc}(\tau)}{\Omega} < \frac{\Gamma_u}{\Omega} \equiv \frac{\pi\omega^4}{2\Omega^3} (25A_1 + 2A_2d^2). \quad (61)$$

This allows us to conveniently bound the time-dependent decoherence rate by a time-independent rate, namely $\Gamma_{eff}(\tau) < \Gamma \equiv \Gamma_{loc} + \Gamma_u$, leading to an upper-bound blurring distance given by

$$\sigma_b(\tau)^2 < \frac{4\Gamma}{\omega} \int_0^\tau d\tau' \eta(\tau')^2. \quad (62)$$

In Fig.1(f), we plot both the original blurring distance (dashed line) and the upper bound (solid line), showing that in the relevant time scale $\tau \approx \tau_m$ the upper bound is a factor of 10 larger than the original blurring distance.

To implement the constant-angle approximation, we need to set two angles: one, ϕ , for $\tau \in [0, \tau_m]$, and a second one, ϕ_2 , for $\tau \in (\tau_m, 2\tau_m]$. As discussed in Sec. 2.5, and observed in Fig.1d, $\phi - \phi_2 = \pi - \delta$, where $0 < \delta \ll 1$ necessitates fine tuning. We choose $\phi = \varphi(\tau_d)$; that is, at the time when $d\varphi(\tau)/d\tau$ is at its first minimum, and we select δ so that the state at $\tau = 2\tau_m$ is closest to the one numerically calculated. For the parameters given in Table 1, this corresponds to $\phi/\pi = \varphi(\tau_d)/\pi \approx 0.499969$ and $\delta/\pi = 7.63944 \times 10^{-6}$.

We are now in a position to analyze how well our analytical approach describes the numerically exact nonlinear dynamics of this particular example.

3.1 Comparison of Analytical Approach with Numerically Exact Results

Following the discussion in Sec. 2.5, we first display in Fig. 2(a) the function $\chi(\tau; \phi)$, as defined in Eq. (49), evaluated for $\tau \in [0, \tau_m]$. The fact that this quantity is small is an indicator of the validity of the constant-angle approximation. More importantly, in Fig. 2(b), we demonstrate the relative errors $\epsilon_n(\tau)$ for the first ($n = 1$) and second ($n = 2$) moments, as defined in Eq. (51) and Eq. (52), for the case of dynamics without decoherence,

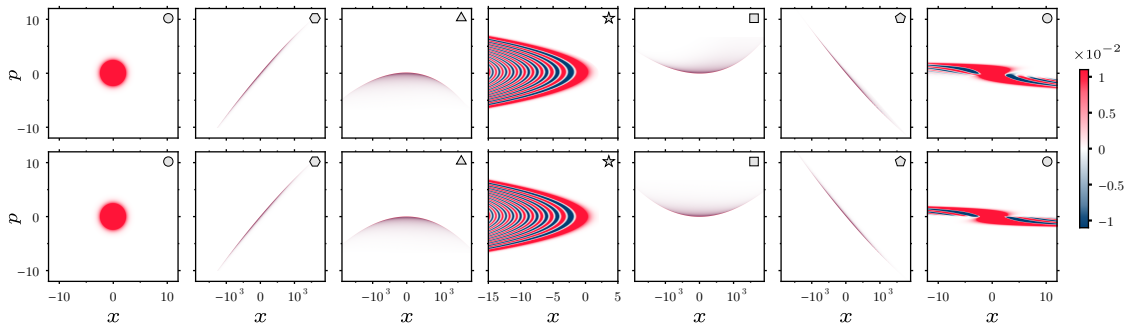


Figure 3: Wigner function of the state of a particle evolving in a double-well potential with parameters given in Table 1 at different instances of time. These instances of time are indicated by polygons and correspond to the times indicated in Fig. 1(a). The first row shows the numerically exact Wigner function $W(\mathbf{r} + \mathbf{r}_c(\tau), \tau)$ obtained using a numerically exact method whereas the second row shows the approximated Wigner function $W_a(\mathbf{r} + \mathbf{r}_c(\tau), \tau)$ obtained using our analytical approach.

which is the most sensitive case. The numerical calculations, performed using the split-operator method [33], reveal relative errors well below one percent, with the exception of the second moments around the turning point $\tau = \tau_m$. This is consistent with the fact that the constant-angle approximation is less accurate around a turning point. This is also evidenced in Fig. 2(a), where the increase of $\chi(\tau; \phi)$ towards the turning point is observable. These results suggest that our analytical approach should yield an excellent approximation of nonlinear open dynamics.

To demonstrate this explicitly, we plot the Wigner function in the centroid frame at the six specific instances of time indicated in Fig. 1a, as shown in Fig. 3. We present both the numerically exact results $W(\mathbf{r} + \mathbf{r}_c(\tau), \tau)$ (which require several hours of computation) and the results using our analytical approach $W_a(\mathbf{r} + \mathbf{r}_c(\tau), \tau)$ (which only require a few minutes). The agreement between the two is remarkably excellent. Furthermore, the cubic-phase states [50, 56–58], generated during the times $\tau \in [0, \tau_m]$, can be obtained analytically. Indeed, one can show, as detailed in App. B.3, that the state in both the centroid and Gaussian frames, in the absence of decoherence during this timescale, can be expressed as follows:

$$W_g^a(\mathbf{r}, \tau) = \frac{1}{\sqrt{2\pi}|\kappa_3(\tau)|^{1/3}} \exp\left[\frac{6\kappa_3(\tau)p_\phi + 1}{12|\kappa_3(\tau)|^2}\right] \text{Ai}\left(\frac{\kappa_3(\tau)x_\phi^2 + p_\phi}{|\kappa_3(\tau)|^{1/3}} + \frac{1}{4|\kappa_3(\tau)|^{4/3}}\right). \quad (63)$$

Here, $\text{Ai}(z)$ denotes the Airy function [59]. For simplification, we have omitted the contribution of $\kappa_4(\tau)$ in Eq. (63), which is negligible for $\tau \leq \tau_m$. The complete expression can be found in App. B.3. Equation (63) indeed represents the Wigner function of a cubic-phase state [50, 56, 57]. Interestingly, the state at $\tau = 2\tau_m$ exhibits a pronounced quartic character. This might seem surprising given that, as we mentioned before, $\kappa_3(\tau) \gg \kappa_4(\tau)$. However, upon inspecting the map $M_{ng}(\tau)$, one realizes that the two contributions of $\kappa_3(\tau)$ and $\kappa_4(\tau)$, corresponding to the first half-orbit ($0 < \tau \leq \tau_m$) and the second half-orbit ($\tau_m < \tau \leq 2\tau_m$), would exactly cancel out or add up for a change in the angle of precisely π (i.e., $\delta = 0$). When δ is small but non-zero, the contribution from $\kappa_4(\tau)$ still accumulates, while the difference of the cubic terms, to first order, contributes another quarticlike term, thereby giving the state at $2\tau_m$ a quartic character.

Finally, an interesting feature of the cubic-phase state generated at $\tau = \tau_m$ is that it produces an interference pattern in the position probability distribution $P(x, \tau) = \int dp W(\mathbf{r}, \tau)$. This is depicted in Fig. 4 for different values of Γ/Ω , using both the numerically exact Q-Xpanse method [31] (dots) and our analytical approach (solid line).

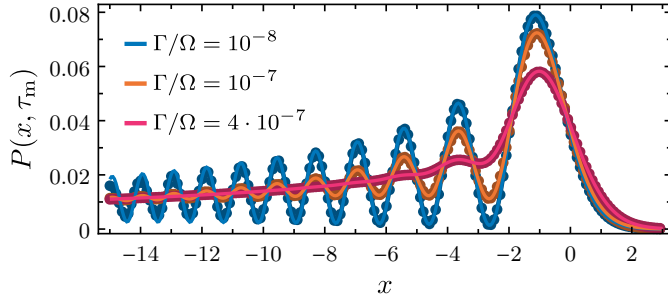


Figure 4: Position probability distribution at time τ_m for a state evolving in a double-well potential for the parameters in Table 1 and for different values of Γ . The lines are computed using the analytical method described in this paper, whereas dots correspond to a numerically exact computation using Q-Xpanse [31].

This demonstrates not only excellent qualitative agreement, but also quantitative, particularly for the first and most relevant interference fringes. With our analytical approach, it can be shown that the interference pattern in the presence of decoherence, $P_a(x, \tau)$, can be expressed as a Gaussian convolution of the interference pattern in the absence of decoherence [42], $P_a^{coh}(x, \tau)$, as follows:

$$P_a(x, \tau) = \frac{1}{\sqrt{2\pi C_{b,xx}(\tau)}} \int dx' \exp\left[-\frac{(x-x')^2}{2C_{b,xx}(\tau)}\right] P_a^{coh}(x', \tau). \quad (64)$$

Here, $C_{b,xx}(\tau)$ is the xx component of the blurring covariance matrix given in Eq. (45), and

$$P_a^{coh}(x, \tau) \equiv \int dp M_c(\tau) M_g(\tau) M_{ng}(\tau) W_g(\mathbf{r}, 0), \quad (65)$$

corresponds to the probability distribution in the absence of decoherence, which is explicitly provided in App. B.4. In addition, the interference pattern in the absence of decoherence can be derived from Eq. (63) and is given by:

$$P_a^{coh}(x, \tau) \propto \exp\left(-\frac{x-x_c(\tau)}{2m_{xp}(\tau)\kappa_3(\tau)}\right) \left| \text{Ai}\left(\frac{x-x_c(\tau)}{m_{px}(\tau)(4\kappa_3(\tau))^{1/3}} + z(\tau)\right) \right|^2. \quad (66)$$

In this equation, $m_{xp}(\tau) = S_{xx}(\tau) \sin(\phi) - S_{xp}(\tau) \cos(\phi)$, and $z(\tau) \in \mathbb{C}$ is a time-dependent function that is given in App. B.4. This analytical expression allows us to derive the scaling of the fringe separation, x_f , which is the distance between the largest interference peak in $P_a(x, \tau_m)$ and its second one. As shown in App. B.4, the fringe separation scales as $x_f \propto |\kappa_3(\tau)|^{1/3}$, or in terms of the physical parameters as $x_f \propto (\Omega/\omega)^{2/3} (1/d)^{1/3}$, for a fixed x_s/d .

4 Conclusions

We have provided an analytical treatment of the Wigner function dynamics for a continuous-variable degree of freedom, such as the position and momentum of a massive particle, in a nonharmonic potential and in the presence of decoherence caused by, among other things, fluctuations of the nonharmonic potential. Our analytical treatment has demonstrated that it can yield an expression of the time-evolved Wigner function that approximates the exact dynamics very accurately, particularly in the case of wide nonharmonic potentials and small fluctuations.

Our analytical method specifically entails performing an exact, suitable reformulation of the open nonlinear dynamical problem via two frame transformations: the classical centroid and the Gaussian frame transformations. In this transformed frame, two approximations can be applied: the key constant-angle approximation and the linearized-decoherence approximation. These approximations facilitate the integration of the dynamical problem and are argued to provide excellent approximations for dynamics that allow the state to expand over scales many orders of magnitude larger than the initial spatial expansion, provided these fluctuations are smaller than the available phase-space that can be explored. In other words, the fluctuations of the state should not occupy the entire available phase-space surface. These requirements define the concept of wide nonharmonic potentials and small fluctuations.

We have tested our analytical method using an example of a massive particle evolving in a wide double-well potential. The method shows excellent agreement with numerical simulations, not just qualitatively, but also quantitatively. In the wide regime, especially in the presence of decoherence, the numerical calculations can be challenging. For these calculations, we utilized a numerical tool, Q-Xpanse, that we recently developed [31]. These numerical calculations often require several hours of computation, while our analytical approach reproduces the results with simple evaluations requiring only a few minutes of calculation. This example is particularly relevant as it has been recently proposed for preparing macroscopic quantum states of a levitated nanoparticle via the generated nonlinear quantum dynamics [32]. The combination of the numerical tool and the analytical method has enabled us to design, optimize, and understand this experimental proposal.

Beyond its utility in modeling experiments, our analytical method also paves the way for interesting research questions that warrant further investigation. Specifically, it would be intriguing to better characterize the dynamical problems in which our method proves effective. It could potentially be utilized to define a class of semiclassical quantum dynamical problems (see e.g., [8, 46]). Furthermore, one could concentrate on the classical regime, either by taking the limit as $\hbar \rightarrow 0$ and studying the efficacy of this method in understanding classical nonlinear dynamics, or by augmenting the strength of the generators of decoherence. In the latter case, it would also be interesting to focus on different types of decoherence, including non-Gaussian decoherence, and apply our method to understand and characterize their effect on the dynamics.

In conclusion, we hope that our analytical approach to understanding open quantum nonlinear dynamics and their classical limit will significantly contribute to this captivating, albeit long-standing, topic.

Acknowledgments

ARC and MRL contributed equally to this work. We thank the Q-Xtreme synergy group for fruitful discussions. This research was supported by the European Union’s Horizon 2020 research and innovation programme under grant agreement No. [863132] (IQLev) and by the European Research Council (ERC) under the grant Agreement No. [951234] (Q-Xtreme ERC-2020-SyG). PTG was partially supported by the Foundation for Polish Science (FNP).

A Explicit expression of the decoherence rates

In the main body of the text, we have reformulated the dissipator due to the fluctuation potential (cf. Eq. (5)) as a double sum with coefficients denoted by Γ_{nm} . To achieve this,

we performed a Taylor expansion of the potential, $V(X)$, as well as its derivative, $V^{(1)}(X)$, in Eq. (4). This led us to the explicit form of the equation:

$$\Gamma_{nm} = \frac{2\pi}{\hbar^2} \frac{X_\Omega^{m+n}}{m!n!} \left[A_1 X_\Omega^2 V^{(m+1)}(0) V^{(n+1)}(0) + A_2 V^{(m)}(0) V^{(n)}(0) \right] + \delta_{n,1} \delta_{m,1} \Gamma_{loc}. \quad (67)$$

These coefficients Γ_{nm} are particularly convenient for expressing the decoherence superoperator within the Hilbert space. However, their translation to the Wigner equation is considerably different, necessitating the introduction of a new set of coefficients denoted as c_{nmk} in Eq. (9). These can be derived by applying the Wigner transform to the decoherence superoperator $\mathcal{D}[\circ]$, resulting in the following equation:

$$c_{nmk} = (-i)^k \left[1 + (-)^k \right] \frac{\Gamma_{nm}}{2\omega} \left[\sum_{q=0}^k (-)^q \binom{n}{k} \binom{m}{k-q} - \binom{m+n}{k} \right]. \quad (68)$$

B Derivations using the the analytical expression of the Wigner function

This appendix is devoted to providing additional details regarding the derivations of analytical expressions for the approximated first and second moments, along with the approximated Wigner function, using the constant-angle approximation; that is, using our main result in Eq. (43). In the derivation, we use the properties

$$\int d\mathbf{r} f(\mathbf{r}) [G[C](\mathbf{r}) \star g(\mathbf{r})] = \int d\mathbf{r} [G[C](\mathbf{r}) \star f(\mathbf{r})] g(\mathbf{r}), \quad (69)$$

$$\int d\mathbf{r} f(\mathbf{r}) g(T^{-1}\mathbf{r}) = \int d\mathbf{r} f(T\mathbf{r}) g(\mathbf{r}) J_T(\mathbf{r}), \quad (70)$$

where \star denotes the convolution,

$$f(\mathbf{r}) \star g(\mathbf{r}) = \int d\mathbf{r}' f(\mathbf{r} - \mathbf{r}') g(\mathbf{r}'), \quad (71)$$

and the Jacobian $J_T(\mathbf{r})$ is the determinant of the matrix

$$\frac{\partial(T\mathbf{r})}{\partial(\mathbf{r})} = \begin{pmatrix} \partial_x(T\mathbf{r})_x & \partial_p(T\mathbf{r})_x \\ \partial_x(T\mathbf{r})_p & \partial_p(T\mathbf{r})_p \end{pmatrix} \quad (72)$$

associated to the transformation T .

B.1 First moments

In the Wigner representation, expectation values of symmetrically-ordered (also Weyl-ordered) operators are computed as phase space integrals. Using our main result in Eq. (43), we find that

$$\boldsymbol{\mu}_a(\tau) \equiv \langle \hat{\mathbf{r}} \rangle_a(\tau) = \int d\mathbf{r} \mathbf{r} D(\tau) M_c(\tau) M_g(\tau) M_{ng}(\tau) W_g(\mathbf{r}, 0). \quad (73)$$

Using the property in Eq. (69) together with the convolution representation of the decoherence map in Eq. (46), one can show that the decoherence map does not contribute the evaluation of the first moments. Moreover, using the property in Eq. (70) for the maps $M_c(\tau)$ and $M_g(\tau)$, and noting that both transformations have unit Jacobian, one arrives to

$$\boldsymbol{\mu}_a(\tau) = \mathbf{r}_c(\tau) + \mathbf{S}(\tau) \int d\mathbf{r} M_{ng}(\tau) W_{nG}(\mathbf{r}, 0). \quad (74)$$

Finally, we note that, in our approximation, the quantum terms included in $M_{ng}(\tau)$ do not contribute to the calculation of the first or second moments. This is a consequence of the fact that the quantum terms include derivatives of order higher than three, which after integration by parts would give no contribution to the integral. Hence, the action of the map $M_{ng}(\tau)$ amounts to a non-linear transformation

$$T\mathbf{r} = \mathbf{r} - \mathbf{R}(\phi)^\top \mathbf{e}_p \sum_{n \geq 3} \kappa_n(\tau) (\mathbf{e}_x^\top \mathbf{R}(\phi) \mathbf{r})^{n-1} \quad (75)$$

which also has unit Jacobian. Hence, combining our previous results and taking the average with the state $W_g(\mathbf{r}, 0)$ we arrive at the result quoted in Eq. (47).

B.2 Covariance matrix

The covariance matrix is computed as the average

$$\begin{aligned} \mathbf{C}_a(\tau) &\equiv \langle (\hat{\mathbf{r}} - \boldsymbol{\mu}(\tau)) (\hat{\mathbf{r}} - \boldsymbol{\mu}(\tau))^\top \rangle(\tau) \\ &= \int d\mathbf{r} (\hat{\mathbf{r}} - \boldsymbol{\mu}(\tau)) (\hat{\mathbf{r}} - \boldsymbol{\mu}(\tau))^\top D(\tau) M_c(\tau) M_g(\tau) M_{ng}(\tau) W_g(\mathbf{r}, 0). \end{aligned} \quad (76)$$

Taking advantage of the property in Eq. (69), we see that the action of the decoherence map is to increase the value of the covariance matrix by $\mathbf{C}_b(\tau)$, as compared to the case without decoherence. Namely, one arrives at

$$\mathbf{C}_a(\tau) = \mathbf{C}_b(\tau) + \int d\mathbf{r} (\hat{\mathbf{r}} - \boldsymbol{\mu}(\tau)) (\hat{\mathbf{r}} - \boldsymbol{\mu}(\tau))^\top M_c(\tau) M_g(\tau) M_{ng}(\tau) W_g(\mathbf{r}, 0). \quad (77)$$

Moreover, similarly to the case of the first moments, taking advantage of Eq. (70) and Eq. (75), one can manipulate the result into the form displayed in Eq. (48).

B.3 State before the turning point in the double-well case

Here, we give more details on how to obtain an analytical expression for the Wigner function in the centroid and Gaussian frame under the constant-angle approximation. To this end, we assume a thermal initial state $W_g(\mathbf{r}, 0)$, which we decompose into Fourier modes as

$$W_g(\mathbf{r}, 0) = \frac{\exp(-x_\phi^2/(2\sigma^2))}{\sqrt{2\pi\sigma^2}} \int \frac{dk_\phi}{2\pi} \exp \left[-(2\bar{n} + 1)k_\phi^2/2 + ip_\phi k_\phi \right]. \quad (78)$$

Applying the evolution map given by the exponential of $\Lambda_{ng}(\tau)$ in Eq. (34) to the state in Eq. (78) leads to an integral expression of the form

$$\frac{1}{2\pi} \int dk \exp \left[i \left(c_3 \frac{k^3}{3} + ic_2 \frac{k^2}{2} + c_1 k \right) \right] = \frac{1}{|c_3|^{1/3}} \exp \left(\frac{c_2^3 + 6c_3 c_2 c_1}{12|c_3|^2} \right) \text{Ai} \left(\frac{c_2^2 + 4c_3 c_1}{4|c_3|^{4/3}} \right), \quad (79)$$

where $c_3 \equiv \kappa_3(\tau) + 3\kappa_4(\tau)x_\phi$, $c_2 \equiv 2\bar{n} + 1 + \sigma_b(\tau)^2$, and $c_1 \equiv p_\phi + \kappa_3(\tau)x_\phi^2 + \kappa_4(\tau)x_\phi^3$ and we have introduced the Airy function

$$\text{Ai}(z) \equiv \frac{1}{2\pi} \int_{-\infty}^{\infty} du \exp \left[i \left(\frac{u^3}{3} + zu \right) \right], \quad (80)$$

for $z \in \mathbb{C}$. Multiplying by the remaining Gaussian in x_ϕ , one can simplify the expression into the final result

$$\begin{aligned}
W_g^a(\mathbf{r}, \tau) &= \frac{1}{\sqrt{2\pi\sigma^2}|\kappa_3(\tau) + 3\kappa_4(\tau)x_\phi|^{1/3}} \\
&\times \exp\left[\frac{(2\bar{n} + 1 + \sigma_b(\tau)^2)^2[6(\kappa_3(\tau) + 3\kappa_4(\tau)x_\phi)(p_\phi + \kappa_3(\tau)x_\phi^2 + \kappa_4(\tau)x_\phi^3)]}{12|\kappa_3(\tau) + 3\kappa_4(\tau)x_\phi|^2}\right] \\
&\times \exp\left[\frac{(2\bar{n} + 1 + \sigma_b(\tau)^2)^3}{12|\kappa_3(\tau) + 3\kappa_4(\tau)x_\phi|^2}\right] \exp\left[-\frac{x_\phi^2}{2\sigma^2}\right] \\
&\times \text{Ai}\left(\frac{(\kappa_3(\tau)x_\phi^2 + \kappa_4(\tau)x_\phi^3 + p_\phi)}{|\kappa_3(\tau) + 3\kappa_4(\tau)x_\phi|^{1/3}} + \frac{(2\bar{n} + 1 + \sigma_b(\tau)^2)^2}{4|\kappa_3(\tau) + 3\kappa_4(\tau)x_\phi|^{4/3}}\right). \tag{81}
\end{aligned}$$

If one sets into the above expression $\kappa_4(\tau) \mapsto 0$, $\sigma_b(\tau) \mapsto 0$, and $\bar{n} \mapsto 0$ it yields the simplified result

$$W_g^a(\mathbf{r}, \tau) = \frac{1}{\sqrt{2\pi}|\kappa_3(\tau)|^{1/3}} \exp\left[\frac{6\kappa_3(\tau)p_\phi + 1}{12|\kappa_3(\tau)|^2}\right] \text{Ai}\left(\frac{\kappa_3(\tau)x_\phi^2 + p_\phi}{|\kappa_3(\tau)|^{1/3}} + \frac{1}{4|\kappa_3(\tau)|^{4/3}}\right), \tag{82}$$

which we show in the main text. Finally, one can move back to the centroid frame by applying $M_g(\tau)$, and to the original frame by applying $M_c(\tau)$. It follows that the approximated Wigner function yields

$$W_a(\mathbf{r}, \tau) = W_g^a(\mathbf{S}(\tau)^{-1}(\mathbf{r} - \mathbf{r}_c(\tau)), \tau). \tag{83}$$

B.4 Interference pattern at the turning point in the double-well case

To obtain the desired probability distribution, we first rewrite x_ϕ and p_ϕ in terms of x and p using the rotation matrix $\mathbf{R}(\phi)$. Then, we apply the map $M_g(\tau)$ to move to the classical trajectory frame, which mixes the coordinates x and p according to the propagator $\mathbf{S}(\tau)^{-1}$. If we denote $f(\mathbf{r}_\phi)$ the function of the right-hand-side of Eq. (82), the Wigner function in the classical trajectory frame is $f(\mathbf{m}(\tau)\mathbf{r})$, where $\mathbf{m}(\tau) \equiv \mathbf{R}(\phi)\mathbf{S}(\tau)^{-1}$, with components $m_{ij}(\tau)$ for $i, j = x, p$. For conciseness of the notation, hereafter we denote $m_{ij}(\tau)$ simply as m_{ij} .

In order to obtain the probability distribution, we have to perform the integral over the variable p , which can be done using the following property of the Airy function (see Ch.3 of [59])

$$\int dy \text{Ai}(y^2 + y_0) \exp(iky) = 2^{2/3} \pi \text{Ai}[2^{-2/3}(y_0 + k)] \text{Ai}[2^{-2/3}(y_0 - k)]. \tag{84}$$

In order to use the property in Eq. (84), we have to rewrite the argument of the Airy function in Eq. (63) without a linear term. To this end, we define

$$y = \frac{1}{\kappa_3(\tau)^{1/6}} \left(\kappa_3(\tau)^{1/2} m_{xp} p + \frac{2\kappa_3(\tau) m_{xp} m_{xx} x + m_{pp}}{2m_{xp} \kappa_3(\tau)^{1/2}} \right), \tag{85}$$

$$y_0(x) = \frac{1}{\kappa_3(\tau)^{1/3}} \left(\frac{m_{xp}^2 - m_{pp}^2 - 4m_{xp} \kappa_3(\tau) x}{4m_{xp}^2 \kappa_3(\tau)} \right), \tag{86}$$

$$k = -i \frac{m_{pp}}{2m_{xp} \kappa_3(\tau)^{4/3}}. \tag{87}$$

Noting that $m_{xx}m_{pp} - m_{xp}m_{px} = 1$, and using y as an integration variable, we can use formula Eq. (84) to compute

$$P_c^a(x, \tau) = \frac{\sqrt{\pi/2}}{|m_{xp}|(\kappa_3(\tau)/2)^{2/3}} \exp \left[\frac{m_{xp}^2 - 3m_{pp}^2 - 6m_{xp}\kappa_3(\tau)x}{12m_{xp}^2\kappa_3(\tau)^2} \right] \times \left| \text{Ai} \left[\frac{1}{(4\kappa_3(\tau))^{1/3}} \left(-\frac{x}{m_{xp}} + \frac{1}{4\kappa_3(\tau)} \left(1 - \frac{m_{pp}^2}{m_{xx}^2} \right) + i\frac{m_{pp}}{2m_{xp}\kappa_3(\tau)} \right) \right] \right|^2. \quad (88)$$

Introducing back the expressions for m_{xx} , m_{xp} , m_{px} and m_{pp} , and shifting $x \mapsto x - x_c(\tau)$ yields the probability $P_a(x, \tau)$.

Let x_f be the distance between the first and second maximum in the fringe pattern defined by Eq. (88). At τ_m , the dependence on the position variable x is scaled with

$$x_f \sim |\kappa_3(\tau_m)|^{1/3} m_{xp}. \quad (89)$$

with $m_{xp} \approx S_{xx}(\tau_m)$, which is only a function of x_s/d . Moreover, one has that

$$\kappa_3(\tau_m) = 3\frac{\omega}{\Omega} \frac{1}{d} \int_0^{\tau_m} d\tau' \eta(\tau')^3 \frac{x_c(\tau')}{d} = 3\frac{\omega}{\Omega} \frac{1}{d} \eta_*^3 \int_0^{\tau_m} d\tau' \frac{\eta(\tau')^3}{\eta_*^3} \frac{x_c(\tau')}{d}. \quad (90)$$

For sufficiently large Ω/ω the integral in Eq. (90) becomes, in very good approximation, also a function of only x_s/d . In that regime, we find that the fringe separation scales with

$$x_f \sim \left(\frac{\Omega}{\omega} \right)^{2/3} \left(\frac{1}{d} \right)^{1/3} f(x_s/d), \quad (91)$$

where $f(x_s/d)$ is an unspecified function of only x_s/d .

References

- [1] E. Schrödinger, *Phys. Rev.* **28**, 1049 (1926).
- [2] M. Born, *Z. Phys.* **38**, 803 (1926).
- [3] W. Heisenberg, *Z. Phys.* **43**, 172 (1927).
- [4] E. Wigner, *Phys. Rev.* **40**, 749 (1932).
- [5] W. P. Schleich, *Quantum optics in phase space* (John Wiley & Sons, Ltd, 2001).
- [6] W. B. Case, *Am. J. Phys.* **76**, 937 (2008).
- [7] E. J. Heller, *J. Chem. Phys.* **65**, 1289 (1976).
- [8] M. V. Berry, *Philos. Trans. Royal Soc. A* **287**, 237 (1977).
- [9] S. Habib, K. Shizume, and W. H. Zurek, *Phys. Rev. Lett.* **80**, 4361 (1998).
- [10] W. H. Zurek, *Nature* **412**, 712 (2001).
- [11] W. H. Zurek, “Decoherence and the transition from quantum to classical — revisited”, in *Quantum decoherence: poincaré seminar 2005* (Birkhäuser Basel, Basel, 2007), pp. 1–31.
- [12] S. Deléglise, I. Dotsenko, C. Sayrin, J. Bernu, M. Brune, J.-M. Raimond, and S. Haroche, *Nature* **455**, 510 (2008).
- [13] M. Hofheinz, H. Wang, M. Ansmann, R. C. Bialczak, E. Lucero, M. Neeley, A. D. O’Connell, D. Sank, J. Wenner, J. M. Martinis, and A. N. Cleland, *Nature* **459**, 546 (2009).

- [14] G. Kirchmair, B. Vlastakis, Z. Leghtas, S. E. Nigg, H. Paik, E. Ginossar, M. Mirrahimi, L. Frunzio, S. M. Girvin, and R. J. Schoelkopf, *Nature* **495**, 205 (2013).
- [15] D. Leibfried, D. M. Meekhof, B. E. King, C. Monroe, W. M. Itano, and D. J. Wineland, *Phys. Rev. Lett.* **77**, 4281 (1996).
- [16] C. Flühmann and J. P. Home, *Phys. Rev. Lett.* **125**, 043602 (2020).
- [17] C. Gonzalez-Ballester, M. Aspelmeyer, L. Novotny, R. Quidant, and O. Romero-Isart, *Science* **374**, eabg3027 (2021).
- [18] U. Delić, M. Reisenbauer, K. Dare, D. Grass, V. Vuletić, N. Kiesel, and M. Aspelmeyer, *Science* **367**, 892 (2020).
- [19] L. Magrini, P. Rosenzweig, C. Bach, A. Deutschmann-Olek, S. G. Hofer, S. Hong, N. Kiesel, A. Kugi, and M. Aspelmeyer, *Nature* **595**, 373 (2021).
- [20] F. Tebbenjohanns, M. L. Mattana, M. Rossi, M. Frimmer, and L. Novotny, *Nature* **595**, 378 (2021).
- [21] M. Kamba, R. Shimizu, and K. Aikawa, *Opt. Express* **30**, 26716 (2022).
- [22] A. Ranfagni, K. Børkje, F. Marino, and F. Marin, *Phys. Rev. Res.* **4**, 033051 (2022).
- [23] J. Piotrowski, D. Windey, J. Vijayan, C. Gonzalez-Ballester, A. de los Ríos Sommer, N. Meyer, R. Quidant, O. Romero-Isart, R. Reimann, and L. Novotny, *Nat. Phys.* **19**, 1009 (2023).
- [24] M. Kamba, R. Shimizu, and K. Aikawa, *arXiv:2303.02831* (2023).
- [25] A. Caldeira and A. Leggett, *Physica A* **121**, 587 (1983).
- [26] W. G. Unruh and W. H. Zurek, *Phys. Rev. D* **40**, 1071 (1989).
- [27] H. Breuer and F. Petruccione, *The theory of open quantum systems* (Oxford University Press, 2002).
- [28] M. E. Gehm, K. M. O'Hara, T. A. Savard, and J. E. Thomas, *Phys. Rev. A* **58**, 3914 (1998).
- [29] S. Schneider and G. J. Milburn, *Phys. Rev. A* **59**, 3766 (1999).
- [30] C. Henkel, S. Pötting, and M. Wilkens, *Applied Physics B* **69**, 379 (1999).
- [31] M. Roda-Llodes, D. Candoli, P. T. Grochowski, A. Riera-Campeny, T. Agrenius, J. J. García-Ripoll, C. Gonzalez-Ballester, and O. Romero-Isart, *arXiv:2306.09083* (2023).
- [32] M. Roda-Llodes, A. Riera-Campeny, D. Candoli, P. T. Grochowski, and O. Romero-Isart, *arXiv:2303.07959* (2023).
- [33] C. Leforestier, R. Bisseling, C. Cerjan, M. Feit, R. Friesner, A. Guldberg, A. Hammerich, G. Jolicard, W. Karrlein, H.-D. Meyer, N. Lipkin, O. Roncero, and R. Kosloff, *J. Comput. Phys.* **94**, 59 (1991).
- [34] L. Dania, D. S. Bykov, F. Goschin, M. Teller, and T. E. Northup, *arXiv:2304.02408* (2023).
- [35] E. Joos and H. D. Zeh, *Z. Phys. B* **59**, 223 (1985).
- [36] M. Schlosshauer, *Decoherence and the quantum-to-classical transition* (Springer-Verlag, Berlin, Heidelberg, 2007).
- [37] O. Romero-Isart, *Phys. Rev. A* **84**, 052121 (2011).
- [38] B. L. Hu, J. P. Paz, and Y. Zhang, *Phys. Rev. D* **45**, 2843 (1992).

- [39] N. Van Kampen, *Phys. Rep.* **24**, 171 (1976).
- [40] V. Jain, J. Gieseler, C. Moritz, C. Dellago, R. Quidant, and L. Novotny, *Phys. Rev. Lett.* **116**, 243601 (2016).
- [41] P. Maurer, C. Gonzalez-Ballester, and O. Romero-Isart, [arXiv:2212.04838](#) (2022).
- [42] O. Romero-Isart, A. C. Pflanzer, F. Blaser, R. Kaltenbaek, N. Kiesel, M. Aspelmeyer, and J. I. Cirac, *Phys. Rev. Lett.* **107**, 020405 (2011).
- [43] J. Bateman, S. Nimmrichter, K. Hornberger, and H. Ulbricht, *Nat. Commun.* **5**, 4788 (2014).
- [44] T. Agrenius, C. Gonzalez-Ballester, P. Maurer, and O. Romero-Isart, *Phys. Rev. Lett.* **130**, 093601 (2023).
- [45] N. Van Kampen, *Physica* **74**, 239 (1974).
- [46] E. J. Heller, *J. Chem. Phys.* **62**, 1544 (1975).
- [47] D. W. Moore and R. Filip, *Comm. Phys.* **5**, 128 (2022).
- [48] O. Romero-Isart, *New J. Phys.* **19**, 123029 (2017).
- [49] H. Pino, J. Prat-Camps, K. Sinha, B. P. Venkatesh, and O. Romero-Isart, *Quantum Sci. Technol.* **3**, 025001 (2018).
- [50] L. Neumeier, M. A. Ciampini, O. Romero-Isart, M. Aspelmeyer, and N. Kiesel, [arXiv:2207.12539](#) (2022).
- [51] T. Weiss and O. Romero-Isart, *Phys. Rev. Res.* **1**, 033157 (2019).
- [52] C. S. Hsu, *Q. Appl. Math.* **17**, 393 (1960).
- [53] A. J. Brizard, *Eur. J. Phys.* **30**, 729 (2009).
- [54] E. T. Whittaker and G. N. Watson, *A course of modern analysis*, 4th ed., Cambridge Mathematical Library (Cambridge University Press, 1996).
- [55] T. Weiss, M. Roda-Llodes, E. Torrontegui, M. Aspelmeyer, and O. Romero-Isart, *Phys. Rev. Lett.* **127**, 023601 (2021).
- [56] C. Weedbrook, S. Pirandola, R. García-Patrón, N. J. Cerf, T. C. Ralph, J. H. Shapiro, and S. Lloyd, *Rev. Mod. Phys.* **84**, 621 (2012).
- [57] M. Brunelli and O. Houhou, *Phys. Rev. A* **100**, 013831 (2019).
- [58] V. Kala, R. Filip, and P. Marek, *Opt. Express* **30**, 31456 (2022).
- [59] O. Vallée and M. Soares, *Airy functions and applications to physics*, 2nd ed. (Imperial College Press, 2010).